Article

Dimethylaniline-Based Hybrid Compounds of Cadmium Diiodide: Synthesis, Crystal Structure, and Physical Properties

Michał Duda,* Marlena Gryl, Andrzej Miniewicz, Marcin Oszajca, Tomasz Seidler, and Wiesław Łasocha*

Read Online

| ACCESS | | Metrics & More | | Article Recommendations | | Supporting Information |

ABSTRACT: In this work, synthesis, crystal structure, and selected properties of two new organic−inorganic compounds based on cadmium iodide with 2,5- and 2,6-dimethylaniline: $CdI_2(2,5\text{-DMA})_2$ **1** and $CdI_2(2,6\text{-DMA})_2$ **2**, respectively, were investigated. Both compounds were obtained using the same methodology, and their crystal structures were determined from powder (**1**) and single-crystal (**2**) X-ray diffraction experiments. The examined materials crystallize in the noncentrosymmetric space group $Fdd2$ and contain large polarizable iodine ions and electron-rich aromatic ligands. Second harmonic generation (SHG) tests performed with urea as a reference revealed high SHG efficiency of powdered samples **1** and **2**. SHG signals measured for samples **1** and **2** are, respectively, around 10 and 8

times larger than the signal for urea. The experimental part was supplemented with theoretical calculations of the second-order electric susceptibility tensor components, $\chi_{ijk}^{(2)}$. Calculated values of the $\chi_{113}^{(2)}$ tensor component around 1.2−1.4 pm·V^{-1} suggest that both materials are relatively efficient second harmonic generators. Fibrous morphology of the materials was revealed by scanning electron microscopy (SEM), and the observed bending of the fibers suggested their significant flexibility. Samples **1** and **2** were also characterized by spectroscopic techniques (IR, RS, UV−Vis-DRS) and their thermal stability and decomposition rates were researched using XRPD and TG/DSC, revealing that both investigated materials are thermally stable up to around 100 °C.
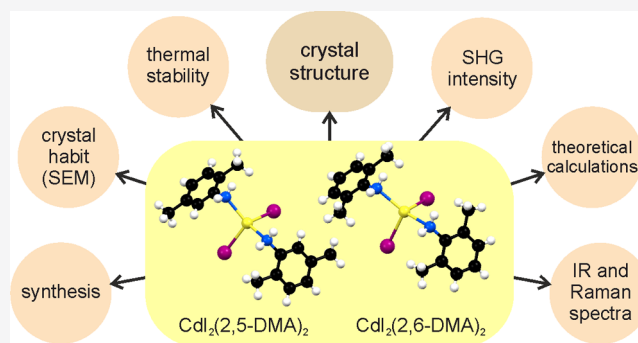
INTRODUCTION

Hybrid organic−inorganic compounds play a significant role in the construction of advanced functional materials due to their structural diversity, mechanical stability enhanced by the inorganic part, and electronic properties provided by organic ligands.[1,2] Such compounds can be designed with various properties in mind, such as catalytic activity, magnetism, electrical conductivity, etc.[3−6] Among the properties exhibited by organic−inorganic compounds, there are nonlinear optical (NLO) effects, the presence of which gives hope for their potential use in optoelectronic devices.[7,8] A particular NLO effect of degenerate sum-frequency generation results in the appearance of the second harmonic light due to annihilation of two photons with a certain frequency, ω, and emission of a single photon with doubled frequency, 2ω.

The technique that has been developed to characterize the efficiency of second harmonic generation (SHG) of newly synthesized materials without growing macroscopic size single-crystals and with minimal time and resource consumption is the Kurtz−Perry SHG powder technique.[9] In this method, the SHG signal is averaged as it is generated by the powder sample with crystallites differently oriented to the excitation light beam.[10] SHG is a second-order NLO effect, and it occurs only

for noncentrosymmetric crystals.[11,12] Many organic compounds and inorganic salts do not show any second-order nonlinear optical effects due to the presence of inversion centers in their crystal structures.[13,14] The same building blocks can be combined in metal−organic frameworks or in co-crystals in a way to ensure noncentrosymmetric structures. Then, the obtained crystals can exhibit the SHG effect.[15−24]

In this work, two new organic−inorganic compounds of cadmium iodide were studied. Some hybrid materials with CdI_2 showing second-order NLO effects are already known;[25] however, there are none with 2,5- and 2,6-dimethylaniline. Cadmium and iodine atoms are characterized by high electron content, and the iodide anion is highly polarizable. In combination with organic ligands, cadmium halides often maintain one-dimensional polymeric structures.[26−33] Rigid inorganic part acts as a perfect template for building functional

materials. On the other hand, the presence of elongated inorganic structural components like chains or ribbons can be problematic as crystals containing those structural components often have needle-shaped habits. Recently, some of us have proven difficulties in studying the nonlinear optical properties of elongated crystals using the Kurtz−Perry technique.[34]

Among the most investigated organic molecules regarding NLO efficiency, there are derivatives of aniline and *N,N*-dialkylaniline.[35] In this study, cadmium iodide was combined with 2,5- and 2,6-dimethylaniline. We decided to use the dimethyl derivatives of aniline because the crystal structure of CdI_2 with unsubstituted aniline, i.e., bis(aniline) cadmium diiodide, has been found centrosymmetric ($C2/c$).[36]

Structural analysis of the synthesized materials, $CdI_2(2,5\text{-}DMA)_2$ (**1**) (from powder diffraction data) and $CdI_2(2,6\text{-}DMA)_2$ (**2**) (from single-crystal XRD data), revealed that these materials crystallize in orthorhombic, noncentrosymmetric $Fdd2$ (No. 43) space group. Polar symmetry of the structures led to the investigation of SHG efficiency in crystalline powder samples of the obtained products using urea compound as a reference. Additionally, theoretical calculations of second-order electric susceptibility tensor components were carried out. The studied materials were also characterized by scanning electron microscopy (SEM), spectroscopic techniques (IR, RS, UV−Vis-DRS), and methods aimed at determining their thermal stability as well as their thermal decomposition routes (nonambient XRPD and TG/DSC).

■ EXPERIMENTAL SECTION

Materials. All chemicals: cadmium iodide (CdI_2) (≥99%, Sigma-Aldrich); 2,5-dimethylaniline (2,5-DMA; $C_8H_{11}N_2$) (99%, Sigma-Aldrich); 2,6-dimethylaniline (2,6-DMA; $C_8H_{11}N_2$) (99%, Sigma-Aldrich); and 2-propanol (PrOH) (pure p.a., POCH, now Avantor) were used as received, without any further purification.

Synthesis. Both materials were synthesized using 50 mmoles of CdI_2, which was dissolved in 40 mL of $PrOH/H_2O$ (1:1) mixture. The obtained solution was stirred and heated (∼70 °C), followed by a dropwise addition of 10 mmoles of the corresponding amine. The precipitating powder product was filtered off, washed three times with 20 mL of $PrOH/H_2O$ (volume ratio 1:1) each time, and dried in air. In the synthesis with 2,6-DMA ligand, colorless, needle-like crystals of the product were found in the filtrate after a few days. Yields for $CdI_2(2,5\text{-}DMA)_2$ **1**: ca. 95% and for $CdI_2(2,6\text{-}DMA)_2$ **2**: ca. 94%. Anal. Calc. Comp. (%) for both compounds: (608.58 g·mol^{-1}): C, 31.58; H, 3.64; N, 4.60. Found: for **1**: C, 31.50; H, 3.52; N, 4.49 and for **2**: C, 31.93; H, 3.56; N, 4.40 (Euro Vector EA 3000 CHNS Elemental Analyzer).

X-Ray Diffraction Measurements. XRPD pattern used for structure solution of **1** was recorded at an X'Pert PRO MPD diffractometer (PANalytical) equipped with a PIXCEL detector, configured in Debye−Scherrer geometry, using CuKα radiation (wavelength: 1.54178 Å) (incident and antiscatter slits of the apertures of 1/4° and 1/2°, respectively; X-ray source: LFF tube; operating power: 40 kV and 30 mA). Sample **1** was packed in a borosilicate glass capillary of 0.3 mm diameter (due to the investigated material's high linear X-ray absorption coefficient). The pattern was recorded at room temperature in the 2θ range of 6−85° with the step size of 0.0131° 2θ.

Diffraction data for a single crystal of **2** were collected at room temperature using the Bruker−Nonius Kappa CCD four circle diffractometer, equipped with a MoKα radiation source and a graphite monochromator.

Nonambient XRPD analyses were performed in air with a HTK Anton Paar chamber (XRK-900) at an X-Pert Philips diffractometer using CuKα radiation. The XRD patterns were recorded every 25 °C

starting from 25 up to 250 °C and every 50 up to 450 °C, with the heating rate of 10 °C·min^{-1}.

Structure Solution. The crystal structure of **1** was determined using the data obtained in the XRPD experiment. Cell parameters, positions of cadmium atoms, and estimated positions of iodine and nitrogen atoms were determined by direct methods using EXPO2014[37] software (indexing was performed with NTREOR program[38]). A complete structure model was built using FOX[39] with the parallel tempering method (a direct space method). Cd and I atoms were fixed in constrained positions and 2,5-DMA molecule was allowed to rotate freely using the available space in the unit cell. Restrained structure refinement was carried out using Jana2006 software[40] with the profile method.[41−43] Rietveld refinement plot is presented in the Supporting Information.

Cell refinement and data reduction for **2** was performed using the firmware Collect (Bruker AXS BV), Denzo and Scalepack.[44] The phase problem was solved by direct methods using SIR-97.[45] All non-hydrogen atoms were refined anisotropically using weighted full-matrix least-squares on F^2. Refinement and further calculations were carried out using SHELXL-2018.[46] The WinGX suite[47] provided a GUI to those programs. The hydrogen atoms joined to carbon atoms were positioned with an idealized geometry and refined using a *riding model* with U_{iso}(H) fixed at 1.2 U_{eq} of C and 1.5 U_{eq} for methyl groups. Hydrogen atoms connected to the nitrogen atom were found on the difference Fourier map and refined with restrained N−H distance to preserve the proper geometry.

The crystallographic data for the investigated compounds were deposited with the Cambridge Crystallographic Data Center (CCDC). The CCDC numbers for the compounds are **1**−2080565, **2**−2151861.

Sample Morphology. Images of the samples in the microscale were obtained using a TESCAN VEGA3 LMU scanning electron microscope with an LaB$_6$ emitter (accelerating voltage: 20 kV). The samples were sputter-coated with gold using a Quorum Q150R coater prior to SEM imaging.

Thermogravimetry and Differential Scanning Calorimetry. Thermogravimetry (TG) and differential scanning calorimetry (DSC) measurements were performed in the air on a Netzsch STA 409 PC Lux system. Twenty milligrams of the samples of the investigated compounds were heated from room temperature to 425 °C. The heating rate was 10 °C·min^{-1}, and the airflow rate was 40 mL·min^{-1}.

UV−Vis Spectroscopy. UV−vis spectra of the studied materials (crystals ground with $BaSO_4$ in proportion 1:1 w/w) were measured in the 200−1100 nm range using a PerkinElmer Lambda 365 spectrometer equipped with a 50 mm Transmission/Reflectance Sphere (slit width: 5 nm, scan speed: 480 nm·min^{-1}).

SHG Measurements. SHG measurements were performed for powdered samples of **1** and **2** using the Kurtz−Perry technique. For SHG excitation, a Q-switched pulse laser (Nd^{3+}:YAG, Surelite II) was used, delivering 10 ns pulses with the repetition rate of 10 Hz, and working at the fundamental wavelength 1064 nm. About 30 individual SHG pulses were measured and averaged for any point of SHG intensity vs laser energy density plot. The unfocused beam of infrared radiation had 5 mm in diameter, and the samples of the studied compounds were confined between two microscope glass plates. The typical crystallite size for both materials was around 100 μm. A fiber optics spectrometer (Qwave, RGB Photonics) collected the green SHG scattered light and measured the spectrum from 300 to 900 nm. The second harmonic signal appeared exactly at λ = 532 nm, and no near resonance effects (e.g., SHG induced luminescence) or spurious light were detected in the spectra. In the experiment, the entrance aperture of the fiber collected only a small portion of the SHG signal, and it was positioned at the angle of 30° to the surface normal. The SHG signal generated for both samples was then compared with the urea standard (grain sizes between 80 and 120 μm). Measurements of SHG intensity in the function of incident laser pulse energy were performed in the range of 20−400 mJ.

Raman Spectroscopy (RS). Raman spectra of the investigated compounds were collected in the range 200−4000 cm^{-1} on a Thermo Scientific Nicolet NXR FT-Raman 9650 spectrometer working at the

wavelength of 1064 nm generated by Nd^{3+}: YAG laser (resolution: 4 cm^{-1}; laser power: 0.5 W) using Thermo Scientific OMNIC v.7.3 program. The measured spectra are shown in the Supporting Information.

Infrared Spectroscopy (IR). Samples **1** and **2** were mixed with nujol (approx. 10% vol.) and placed in IR cells made of KRS-5 windows. The spectra (100 scans; resolution of 2 cm^{-1}) were recorded at room temperature ranging from 420 to 4000 cm^{-1} using Bruker Equinox 55 spectrometer equipped with an MCT detector. The collected spectra are available in the Supporting Information.

■ RESULTS AND DISCUSSION

Crystal Structure Description. Both **1** and **2** crystallize in the orthorhombic crystal system in the $Fdd2$ space group (No. 43). Volumes of the unit cell and the corresponding cell parameters for **1** and **2** are similar (Table 1).

Table 1. Selected Crystallographic Data for $CdI_2(2,5-DMA)_2$ 1 and $CdI_2(2,6-DMA)_2$ 2

	1	2
empirical formula	$CdI_2C_{16}H_{22}N_2$	$CdI_2C_{16}H_{22}N_2$
formula weight $(g \cdot mol^{-1})$	608.6	608.6
crystal system	orthorhombic	orthorhombic
space group	$Fdd2$	$Fdd2$
a (Å)	27.0117(7)	25.9670(2)
b (Å)	31.4906(11)	33.1940(4)
c (Å)	4.5366(2)	4.4890(6)
V ($Å^3$)	3858.9(2)	3869.3(5)
Z	8	8

The unit cell has a form of a thin cuboid—the a and b periods are relatively long, while the c period is much shorter.

In both structures, each cadmium atom is coordinated by two DMA molecules and surrounded by four iodine anions: two I1 atoms at a distance around 2.78 Å for **1** and 2.86 Å for **2** and two I2 atoms at a greater distance: ~3.62 Å in **1** and ~3.29 Å in **2** (Figure 1, full lists of distances are in the Supporting Information).
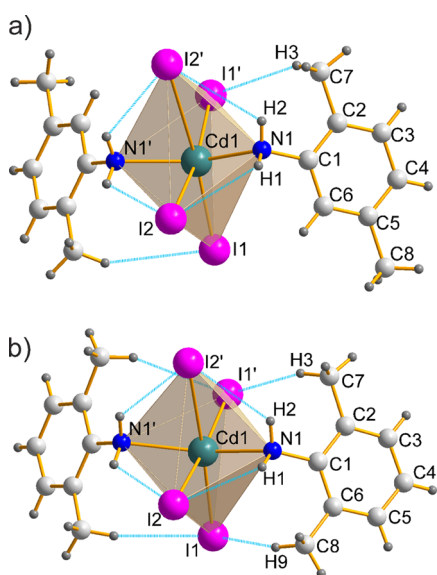
Figure 1. Coordination environment of cadmium ion in: (a) $CdI_2(2,5-DMA)_2$ **1**; (b) $CdI_2(2,6-DMA)_2$ **2**; D−H···A interactions are shown as bright blue lines.

A distorted coordination octahedron is created around each Cd with the amine groups from the substituted aniline molecules (Cd−N ∼ 2.29 Å for **1** and ∼2.38 Å for **2**). Iodine anions form the octahedron's equatorial plane. The two vertices of the octahedron are occupied by nitrogen atoms of the corresponding aniline derivative. The most likely interactions responsible for the formation of such units are N−H···I interactions between the hydrogen atoms of amine groups coordinating cadmium and iodine ions (Table 2).

A direct comparison of the coordination spheres in **1** and **2** (available in the Supporting Information) indicates that their geometries are very similar.

By sharing two adjacent edges of the equatorial plane, the coordination polyhedrons form simple, infinite ribbons. Projection of the crystal structure of **1** along [010] shown in Figure 2a reveals the ribbons propagating in the [001] direction.

In total, eight ribbons with organic ligands on both sides of them pass through each unit cell (Figure 2b). The methylaniline molecules are attached at an angle of around 50° to the $[CdI_2]_n$ ribbons. Distances between centroids of aromatic rings of the neighboring amine molecules from the same side of a ribbon are 4.54 Å for **1** and 4.49 Å for **2**. In contrast, the distances between the centroid of the aniline ring and the nitrogen atom of the adjacent molecules are about 3.73 and 3.80 Å, respectively. More crystallographic data and details of the refinement procedure are presented in the Supporting Information.

SEM. SEM images of samples of the investigated compounds, shown in Figure 3, revealed that both materials are built of elastic fibers with diameters from 4.8 to 12.2 μm for **1** and 19.5−98 μm for **2**.

Closer observation shows that the fibers of **1** do not have a tendency to aggregate, while for **2** the observed fibers usually consist of multiple thinner ones (as seen in Figure 3f).

Thermal Stability. XRPD patterns measured in the nonambient conditions for compounds **1** and **2** are collected in Figure 4. These graphs in the 3-D form and phase analysis of the decomposition products are available in the Supporting Information. Both the investigated compounds exhibit thermal stability up to the temperature of 100 °C. Above this value (125−350 °C), they decompose, and cadmium iodide (PDF card number: 00-033-0239[48]) is the sole crystalline phase present in the samples, though hints of amorphous content may be detected in the 25−30° 2θ range. In **1**, the CdI_2 phase has higher crystallinity than **2**, except the maximum located around 42.5° 2θ. Above temperatures 350−400 °C the XRD patterns are almost flat, and only few maxima with a small intensity of Al_2O_3 support (PDF card number: 00-001-1305[48]) appear in the pattern.

Simultaneous TG and DSC plots for the investigated compounds are shown in Figure 5. Interpretation of the measurements is presented in Table 3.

In the TG curve for both materials **1** and **2**, there is a two-step decrease of sample weight, which can be attributed directly to the removal of molecules of dimethylaniline. The weight loss for compound **1** starts at a higher temperature than for **2**. The two steps in TG are reflected in DSC curves. At high temperatures, up to 425 °C, the sample weight is almost stable. However, an additional sharp valley appears in the DSC plots at the same temperature of ∼385 °C for both materials. Since this decrease is not accompanied by any changes in the sample weight, it could possibly be related to melting of cadmium

Table 2. The Geometry of D−H···A Bonds within the Coordination Environment of Cd in CdI$_2$(2,5-DMA)$_2$ 1 and CdI$_2$(2,6-DMA)$_2$ 2^a

compound code	H-bond	distance (Å)			D−H−A angle (°)
		D−H	H···A	D−A	
1	N1−H1···I2$^{(i)}$	0.87(2)	3.07(1)	3.689(17)	130(1)
	N1−H2···I2′$^{(ii)}$	0.87(1)	3.15(1)	3.696(16)	123(1)
	C7−H3···I1′$^{(iii)}$	0.96(2)	3.14(1)	4.015(15)	152(1)
2	N1−H1···I2$^{(iv)}$	0.94(5)	2.93(5)	3.588(5)	129(4)
	N1−H2···I2′$^{(v)}$	0.94(7)	2.87(8)	3.582(5)	133(6)
	C7−H3···I1′$^{(vi)}$	0.96(1)	3.09(1)	3.961(8)	152(1)
	C8−H9···I1$^{(vii)}$	0.96(1)	2.99(1)	3.892(8)	158(1)

^{a}Symmetry codes: *(i) 0.25 − x; −0.75 + y; 0.25 + z; (ii) 0.25 + x; 1.25 − y; 0.25 + z; (iii) 0.25 + x, 1.25 − y, −0.75 + z; (iv) 0.5 − x, 0.5 − y, 1 + z ; (v) x, y, 1 + z; (vi) x, y, z;(vii) 0.5 − x, 0.5 − y, z.*
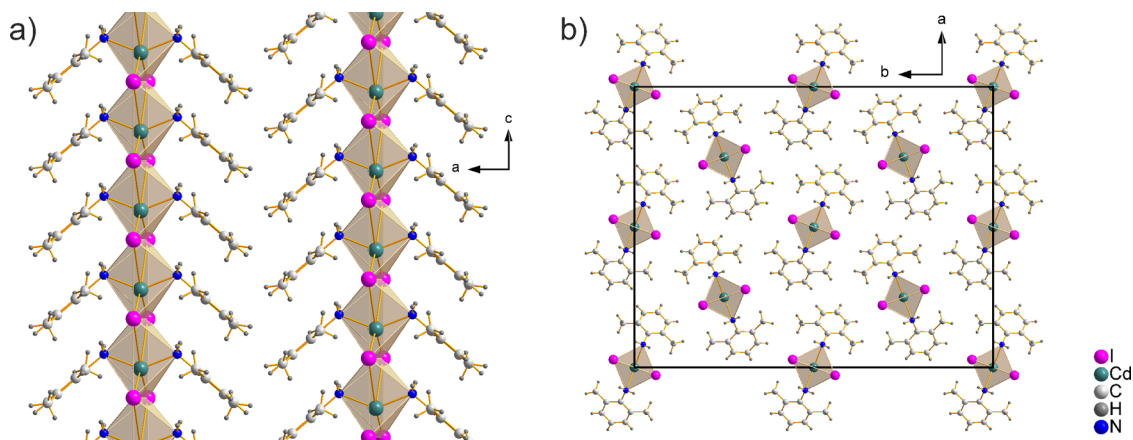
Figure 2. (a) Projection of the crystal structure of CdI$_2$(2,5-DMA)$_2$ **1** along the [010] direction; (b) packing of the structural components in the unit cell (shown as a black rectangle) of CdI$_2$(2,6-DMA)$_2$ **2** shown along the [001] direction.
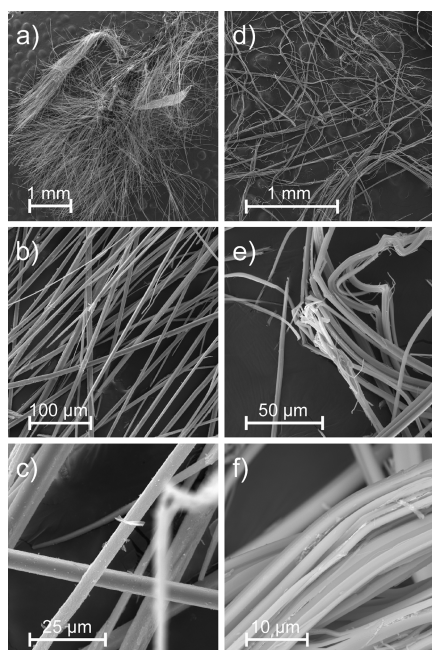
Figure 3. SEM images of as grown compounds: CdI$_2$(2,5-DMA)$_2$ **1** (a,b,c); and CdI$_2$(2,6-DMA)$_2$**2** (d,e,f).

iodide (m.p. of CdI$_2$ ∼ 387 °C). Differences between XRD and TG/DSC results could be explained by the heating programs used in the two methods. In the XRPD method, the XRD patterns were registered a few minutes after reaching the appropriate temperature of the samples.

Second Harmonic Generation. Both obtained materials crystallize in a polar space group, *Fdd*2, and can exhibit nonlinear optical properties of second-order, e.g., second harmonic generation (SHG). To assess the magnitude of the effect, we have performed calculations of static second-order susceptibility tensor components $\chi_{ijk}^{(2)}$ for the crystal structures of **1** and **2**. Experimentally determined crystal structure was optimized using PB3LYP functional and all-electron POB-TZVP basis set for Cd and I and 6-311Gdp for the remaining atoms. Calculations were performed in Crystal17 software.[49,50] Electric susceptibility tensors and refractive indices were calculated using the modified local field theory (LFT)[51,52] approach introduced by Munn et al.[53−55] The calculations for the molecular (2,5-DMA and 2,6-DMA) and ionic building blocks (Cd^{2+}, I$^−$) were carried out in Gaussian09.[56] For the sake of comparison, for the structure of **2** we have selected the complex CdI$_2$(2,6-DMA)$_2$ as the molecular component. Static polarizabilities were calculated at the MP2/def2-TZVP level. The frequency dispersion was introduced with B3LYP/def2-TZVP. The partitioning of the molecular/ionic polarizabilities into the atomic contributions was performed in AIMAll.[57]

The obtained results are presented in Table 4. Crystals of **2** exhibit almost identical maximum birefringence at 532 nm wavelength (Δn = 0.081) and $\chi^{(2)}$ tensor components as that of **1** (Δn = 0.08). The axis of the optical indicatrix that can be related to n_γ refractive index coincides with the [010] direction. The smallest n_α refractive index can be found
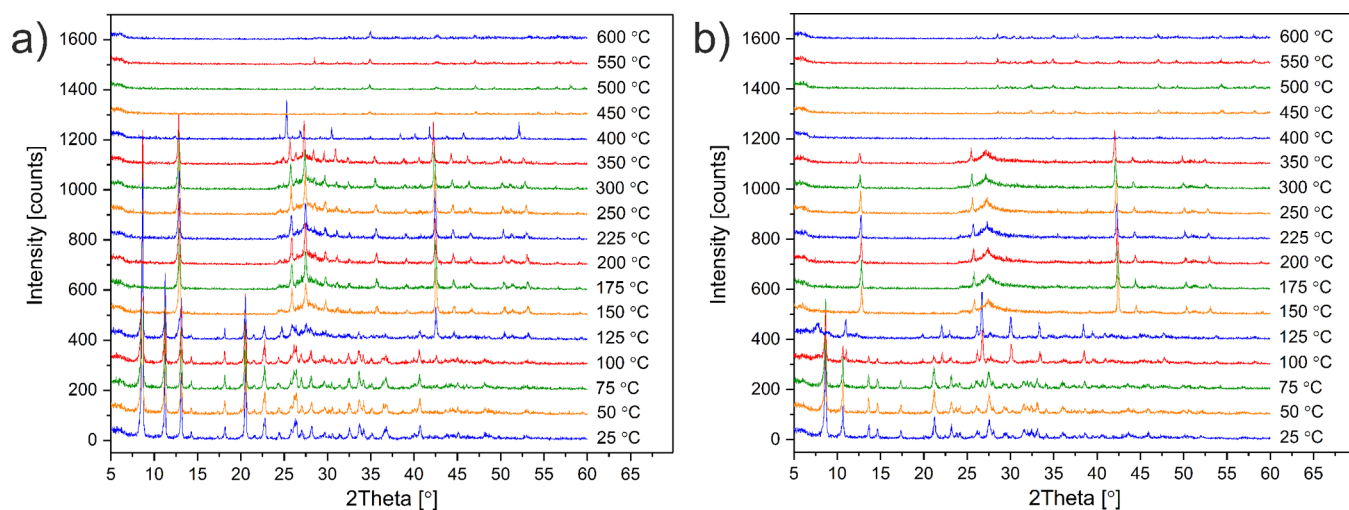
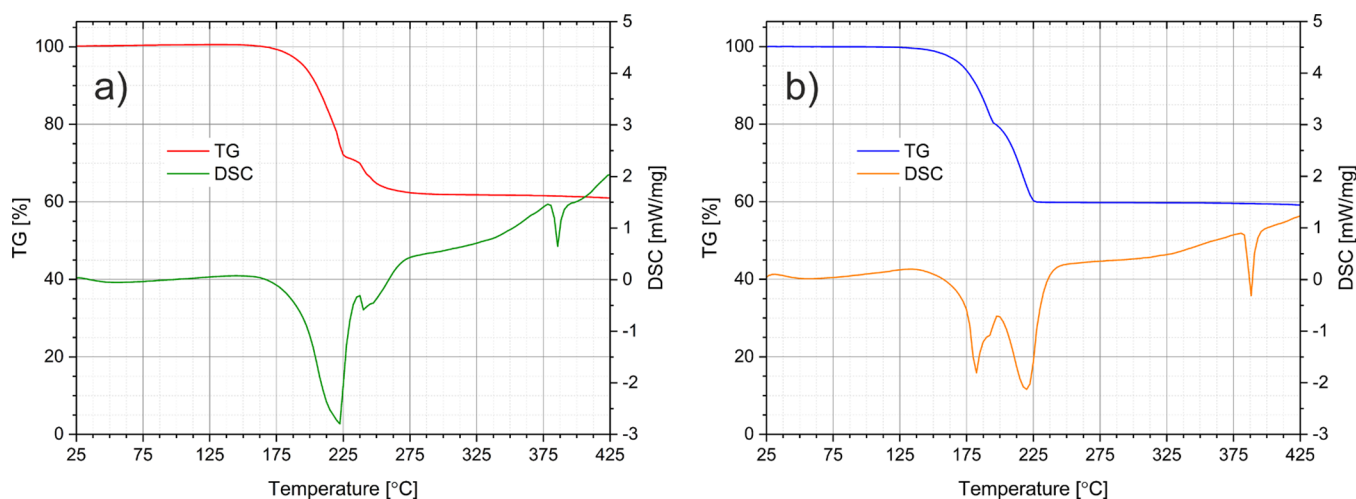**Figure 4.** Nonambient XRPD patterns for: (a) $CdI_2(2,5\text{-DMA})_2$ **1**; (b) $CdI_2(2,6\text{-DMA})_2$ **2**.

Figure 5. TG and DSC plots for: (a) $CdI_2(2,5\text{-DMA})_2$ **1**; (b) $CdI_2(2,6\text{-DMA})_2$ **2**.

Table 3. TG Weight Loss for $CdI_2(2,5\text{-DMA})_2$ 1 and $CdI_2(2,6\text{-DMA})_2$ 2

compound code	temperature range (°C)	weight loss (wt %)[a]	lost species	total mass released (%)[b]	final product
1	150−225	28.0	2,5-DMA	38.7	CdI_2
	225−290	10.7	2,5-DMA		
2	125−190	19.4	2,6-DMA	40.0	CdI_2
	190−225	20.6	2,6-DMA		

[a]Calculated weight loss for one half of the total number of molecules of amine in the samples: 19.9%. [b]Calculated weight loss for all molecules of the corresponding amine: 39.8%.

along [001] direction, where we can see the propagation of the ribbons mentioned in the Crystal Structure Description. The intermediate n_β can be measured along the crystallographic x-axis, where the ribbons are connected via C−H···π interactions. This particular packing of structural components is responsible for the needle shape of those crystals, revealed in SEM images, unfavorable for optical property measurements. In the case of the ionic approach the highest values of the $\chi_{113}^{(2)}$ tensor component are ca. 1.2−1.4 pm·V^{-1}, what suggests that both materials could be considered as relatively efficient SH generators (compare d_{36} for KDP equal to 0.35 pm·V^{-1} for

KDP). This model is of course a simplification as some Cd−I interactions can be considered more ionic and other more dative in nature. It is reasonable to assume that the $\chi_{ijk}^{(2)}$ tensor components are actually higher than those reported for the assumed ionic models and lower than the polymeric ones. This is in agreement with the experimental observations.

Experimental plots of SHG signal intensity versus wavelength are shown in Figure 6. The maximum intensity is measured at 532 nm what is half of the wavelength of the incident laser beam 1064 nm. SHG signals have shown parabolic dependence on laser pulse energy. To calculate the effective nonlinear susceptibility tensor components, the square root of SHG signal versus input pulse energy was plotted (as insets in Figure 6). By comparing the obtained slopes of the linear dependences for **1** and **2** with that of the slope for the reference powder of urea (measured in the same conditions), the values of averaged $d_{ijk}^{(2)}$ could be obtained. Taking into account that the dominant tensor element for urea is d_{14} = 1.4 pm·V^{-1},[11] $d_{eff}^{(2)}$ values of 4.54 pm·V^{-1} for **1** and 4.14 pm·V^{-1} for **2** can be estimated. However, it needs to be stressed that these experimental results are loaded with high error, related with the sample properties (especially the needle-like habit of the crystallites contributing to significant

Table 4. Electric Susceptibility Tensor Components $\chi^{(2)}_{ijk}$ in pm·V^{-1} Calculated for CdI$_2$(2,5-DMA)$_2$ 1 and CdI$_2$(2,6-DMA)$_2$ 2; n_α, n_β, and n_γ Are Refractive Indices

compound code	λ (nm)	n_α	n_β	n_γ	$\chi^{(2)}_{113}$	$\chi^{(2)}_{311}$	$\chi^{(2)}_{223}$	$\chi^{(2)}_{322}$	$\chi^{(2)}_{333}$
1	∞	1.498	1.551	1.572	1.0	1.0	−0.3	−0.3	0.4
	1064	1.503	1.558	1.579	1.2	1.2	−0.3	−0.3	0.4
	532	1.521	1.582	1.601					
1*[a]	∞	1.638	1.689	1.795	−2.4	−2.4	−1.7	−1.7	−8.2
	1064	1.649	1.703	1.821	−4.7	−0.4	−2.3	−2.2	−12.5
	532	1.689	1.750	1.928					
2	∞	1.496	1.550	1.579	1.1	1.1	0.3	0.3	−0.4
	1064	1.502	1.557	1.586	1.3	1.4	0.4	0.4	−0.5
	532	1.519	1.580	1.609					
2*[b]	∞	1.652	1.711	1.712	−2.2	−2.2	−1.8	−1.8	−12.4
	1064	1.667	1.728	1.737	−6.2	6.8	−4.5	−1.7	−20.4
	532	1.729	1.793	1.862					

[a]1* CdI$_2$(2,5-DMA)$_2$ treated as the molecular component in the calculations. [b]2* CdI$_2$(2,6-DMA)$_2$ treated as the molecular component in the calculations.
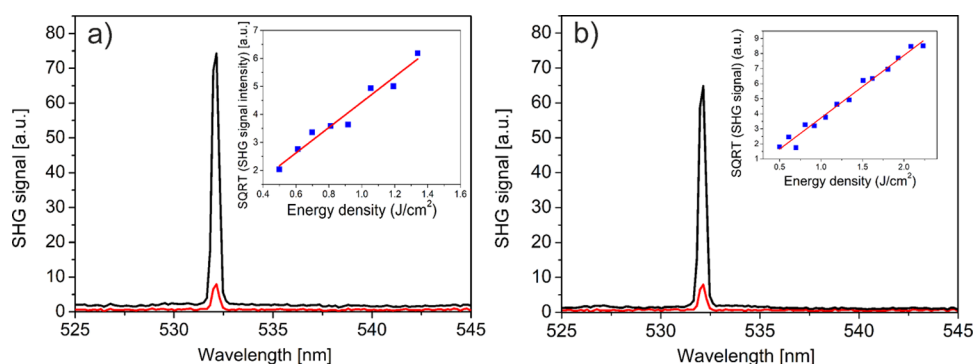
Figure 6. Comparison of SHG signals for powdered samples of (a) CdI$_2$(2,5-DMA)$_2$ **1** and (b) CdI$_2$(2,6-DMA)$_2$ **2** (in black) with urea reference (in red) with inserted square root of SHG intensity vs pulse energy density; SHG signals for the investigated compounds and urea were measured in identical irradiation conditions (at laser energy density of 0.28 J·cm^{-2}) and geometry of light collection.
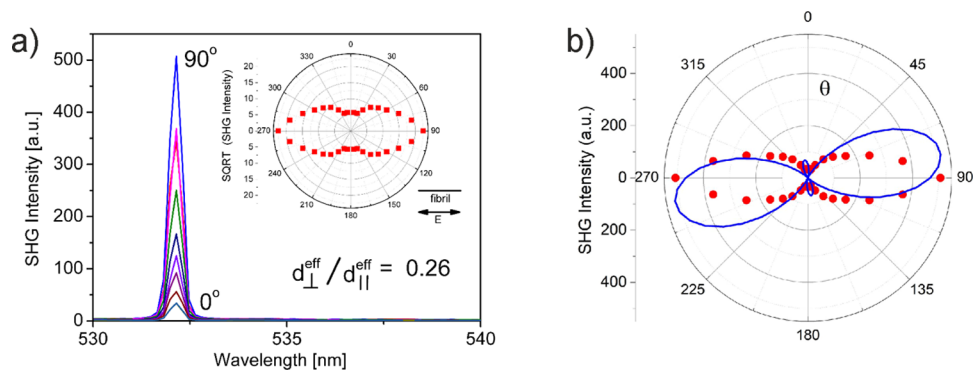
Figure 7. (a) SHG response for CdI$_2$(2,6-DMA)$_2$ **2** observed during rotation of bunch of fibrils with respect to linear polarization of Nd$^+$:YAG laser beam. The ratio of square roots of SHG intensities measured for incident light polarization along the fibrils (∥) and perpendicular to them (⊥) equals 0.26 and it reflects the difference between the dominant tensor component $d^{(2)}_{333}$ and $d^{(2)}_{113}$ or $d^{(2)}_{223}$; (b) comparison of angular dependence of SHG intensity measured for **2** and calculated from $\langle d^{(2)}_{eff}(\theta)\rangle^2$ on the basis of eq 3 and theoretical values reported in Table 4 for **2***.

anisotropy of optical properties, but also crystallite size, fiber tendency to aggregation, etc.).

In Figure 3, there are SEM images of the investigated compounds showing their tendency to grow in the form of fibers with diameters from 4.8 to 12.2 μm for **1** and 19.5−98 μm for **2**. Such diameters are comparable or larger than the coherence lengths l_c for these materials. Coherence lengths l_c for SHG process depend inversely on refractive index difference and their dispersion:[58]

$$l_c = \frac{\pi}{\Delta k} = \frac{\lambda_\omega}{4(n_{2\omega} - n_\omega)} \tag{1}$$

where $n_{2\omega}$ and n_ω are refractive indices of the investigated crystals at frequencies 2ω and ω corresponding to the used in experiment wavelengths 532 and 1064 nm, respectively. Using the calculated values of refractive indices listed in Table 4, the coherence lengths were estimated as $l_c \approx 2.7$ μm for the crystal **1** and $l_c \approx 3.4$ μm for the crystal **2**, respectively. Thus, it can be safely assumed that SHG response is not measured under strict

phase matching conditions. For the SHG anisotropy experiment, we carefully prepared the axially aligned bunch of fibers for the compound **2** and fixed it on a glass plate mounted on a rotatory stage. Then, the bunch was excited with pulses of linearly polarized light and SHG intensities scattered from the sample that was rotated over 360° range with 10° steps were measured. In order to avoid heat accumulation, after the collection of 30 intensities during the interval of 3 s, we waited for 3 min to allow the sample to relax before the next measurement. No polarizer was placed before the spectrometer entrance fiber. Quite a large anisotropy of SHG response during rotation was observed. The results of these measurements are shown in Figure 7a.

The polar plot of square root of the measured SHG intensity is proportional to the effective nonlinear coefficient $d_{eff}^{(2)}$ that can be calculated for the $mm2$ point group under Kleinman conditions as

$$d_{eff}^{(2)}(\theta) = d_{311}^{(2)}\cos^2\theta + d_{333}^{(2)}\sin^2\theta + 2 \cdot d_{113}^{(2)} \cdot \sin\theta \cdot \cos\theta \qquad (2)$$

where θ describes the angle between electric field of incoming light at a frequency ω with respect to normal to the long axis of the fiber; note that $d_{ijk}^{(2)} = \frac{1}{2} \cdot \chi_{ijk}^{(2)}$. Deriving the above equation for the $mm2$ point group we assumed that irradiating light **k**-vector incoming perpendicularly to the sample plane is parallel to the y-axis and fibers rotate in the (x,z) plane. However, any individual fiber can be randomly oriented with respect to its rotation around its own axis. Therefore, we took into account also this type of disorder and using the values of susceptibility tensor components for compound **2*** from Table 4 theoretical $d_{eff}^{(2)}(\theta)$ polar dependence was calculated from the formula including algebraic averaging in the following form:

$$\langle d_{eff}^{(2)}(\theta)\rangle = d_{311}^{(2)}\cos^2\theta + d_{333}^{(2)}\sin^2\theta$$
$$+ 0.5 \cdot [(2 \cdot d_{113}^{(2)} + 2 \cdot d_{223}^{(2)}) \cdot \sin\theta \cdot \cos\theta] \qquad (3)$$

Knowing the $\langle d_{eff}^{(2)}(\theta)\rangle$, we could calculate the polar plot based on the fact that intensity of SHG depends quadratically on $\langle d_{eff}^{(2)}(\theta)\rangle$. The direct comparison of the experimentally measured polarimetric dependence of SHG intensity with that predicted theoretically (see Table 4, the row corresponding to 1064 nm for compound **2***) is shown in Figure 7b. Shapes are similar, though in the experiment two small loops perpendicular to the main ones were not observed, probably due to disorder in the fibers bunch. The values of the main tensor coefficients calculated as the molecular components in this hybrid organic−inorganic crystal are approximately two times larger than experimentally observed (theoretical value for $d_{333}^{(2)} = 10.2$ pm·V^{-1} whereas the experimental one $<d_{eff,\ exp}^{(2)}> \approx 4.14$ pm·V^{-1}). The experimental values are in between those calculated theoretically 10.2 and 0.7 pm·V^{-1} by molecular approach and ionic model, respectively.

The materials designed for SHG application should meet special requirements beyond high nonlinear optical susceptibility values, such as stability and optical transparency in the operational wavelength.[59,60] The optical damage threshold is moderate and for **1** it was observed at 1.4 J·cm^{-2} while for **2** at 2.2 J·cm^{-2}. Taking into account that the laser pulse duration was 10 ns, it gives 140 and 220 MW·cm^{-2}, respectively. The damage thresholds were determined by observing the departure of SHG intensity versus energy density from the parabolic behavior and the darkening of the material. The

optical damage thresholds for urea 1.5 GW·cm^{-2} and that of KDP amounting to 0.2−10 GW·cm^{-2} are larger.[61] The thresholds of **1** and **2** are, however, higher than for another compound of cadmium iodide reported in a recent paper co-authored by one of us,[62] where the threshold is equivalent to power density of 100 MW·cm^{-2}.

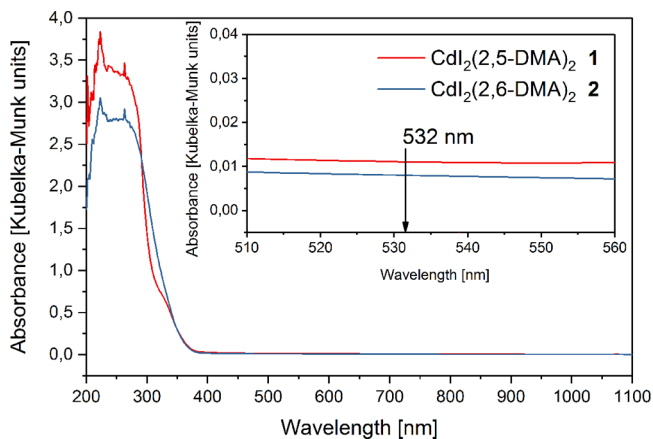Figure 8 shows the UV−vis spectra of **1** and **2** measured in the range 200−1100 nm.

Figure 8. UV−vis spectra of the investigated compounds.

Both investigated materials do not absorb light in the range 400−1100 nm and, because of that, the SHG signal can achieve the maximum intensity in that region.

■ SUMMARY

In this research, we determined and described crystal structures of two novel organic−inorganic materials composed of cadmium iodide and dimethyl derivatives of aniline. Both compounds crystallize in the $Fdd2$ space group and are composed of ribbons containing iodine anions and cadmium cations, to which the organic ligands are linked. The a and b unit cell parameters are much longer than that of c, which results in fibrous morphology of the obtained crystals.

Both $CdI_2(2,5\text{-}DMA)_2$ and $CdI_2(2,6\text{-}DMA)_2$ were found to be optically stable and their SHG signal is greater than that of urea reference. For comparison, the SGH signal of a compound of cadmium sulfate with m-phenylenediamine reported by our team in 2018[1] is 8 times lower than the signal of KDP and for the same experimental conditions the SHG response for KDP is 9 times smaller than that for urea powder. The investigated compounds are also easy to obtain as powders, thermally stable under normal conditions (up to around 100 °C), transparent in the visible region of the spectrum, and sparingly soluble in water.

Radhakrishnan[60] indicates that an important feature of materials designed for NLO applications is the possibility of fabricating thin films with orientationally ordered crystallites. It was shown that the crystal structures of both compounds are built of parallel polymeric chains what makes them likely to comply with this condition, but more detailed research is needed, including proper technique of thin film preparation instead of growing separate fibers.

■ ASSOCIATED CONTENT

Ⓢ Supporting Information

The Supporting Information is available free of charge at https://pubs.acs.org/doi/10.1021/acs.cgd.2c00191.

> Structural data (structure refinement, atomic distances and angles) for **1** and **2**. Raman spectra of **1** and **2**. IR spectra of **1** and **2**. Nonambient powder diffraction patterns of **1** and **2** plotted in a 3-D graph. Phase analysis of products of thermal decomposition of samples **1** and **2**. Structure of **1** optimized in Crystal17 superimposed on the structure refined in Jana2006. Calculated size of bandgaps for **1** and **2** (PDF)

Accession Codes

CCDC 2080565 and 2151861 contain the supplementary crystallographic data for this paper. These data can be obtained free of charge via www.ccdc.cam.ac.uk/data_request/cif, or by emailing data_request@ccdc.cam.ac.uk, or by contacting The Cambridge Crystallographic Data Centre, 12 Union Road, Cambridge CB2 1EZ, UK; fax: +44 1223 336033.

■ AUTHOR INFORMATION

Corresponding Authors

Michał Duda − *Faculty of Chemistry, Jagiellonian University, 30-387 Kraków, Poland;* ⓘ orcid.org/0000-0001-5186-6435; Email: michal.duda@uj.edu.pl

Wiesław Łasocha − *Faculty of Chemistry, Jagiellonian University, 30-387 Kraków, Poland; Jerzy Haber Institute of Catalysis and Surface Chemistry, Polish Academy of Sciences, Kraków 30-239, Poland;* ⓘ orcid.org/0000-0001-7083-1860; Email: lasocha@chemia.uj.edu.pl

Authors

Marlena Gryl − *Faculty of Chemistry, Jagiellonian University, 30-387 Kraków, Poland*

Andrzej Miniewicz − *Advanced Materials Engineering and Modelling Group, Faculty of Chemistry, Wrocław University of Science and Technology, 50-370 Wrocław, Poland;* ⓘ orcid.org/0000-0003-2470-6246

Marcin Oszajca − *Faculty of Chemistry, Jagiellonian University, 30-387 Kraków, Poland;* ⓘ orcid.org/0000-0001-8769-8023

Tomasz Seidler − *Faculty of Chemistry, Jagiellonian University, 30-387 Kraków, Poland*

Complete contact information is available at: https://pubs.acs.org/10.1021/acs.cgd.2c00191

Author Contributions

The manuscript was written through contributions of all authors. All authors have given approval to the final version of the manuscript.

Notes

The authors declare no competing financial interest.

■ ACKNOWLEDGMENTS

■ ABBREVIATIONS

DMA, dimethylaniline; XRD, X-ray diffraction; XRPD, X-ray powder diffraction; SEM, scanning electron microscopy; NLO, nonlinear optical (properties); SHG, second harmonic generation; TG, thermogravimetry; DSC, differential scanning calorimetry; RS, Raman spectroscopy; IR, infrared (spectroscopy); UV−vis-DRS, ultraviolet−visible diffusive reflectance spectroscopy.

■ REFERENCES

(1) González Guillén, A.; Oszajca, M.; Luberda-Durnaś, K.; Gryl, M.; Bartkiewicz, S.; Miniewicz, A.; Lasocha, W. Synthesis, Characterization, and Optical Properties of Organic−Inorganic Hybrid Layered Materials: A Solvent-Free Ligand Controlled Dimensionality Approach Based on Metal Sulfates and Aromatic Diamines. *Cryst. Growth Des.* **2018**, *18*, 5029−5037.

(2) Ostrowska, K.; Musielak, B.; Szneler, E.; Dudek, Ł.; Gryl, M.; Stadnicka, K. Chelate Ring Size Effect as a Factor of Selective Fluorescent Recognition of Zn^{2+} Ions by Pyrrolo[2,3-b]Quinoxaline with a Substituted 2-Pyridyl Group Receptor. *Inorg. Chem.* **2015**, *54*, 8423−8435.

(3) Mitzi, D. B. Synthesis, Structure, and Properties of Organic-Inorganic Perovskites and Related Materials. *Prog. Inorg. Chem.* **1999**, *48*, 1−121.

(4) Bożek, B.; Neves, P.; Valente, A. A.; Łasocha, W. Ionic ammonium and anilinium based polymolybdate hybrid catalysts for olefin epoxidation. *Appl. Catal. A, Gen.* **2018**, *564*, 13−25.

(5) Zhao, Y.; Wu, H.; Emge, T. J.; Gong, Q.; Nijem, N.; Chabal, Y. J.; Kong, L.; Langreth, D. C.; Liu, H.; Zeng, H.; Li, J. Enhancing Gas Adsorption and Separation Capacity through Ligand Functionalization of Microporous Metal−Organic Framework Structures. *Chem. − Eur. J.* **2011**, *17*, 5101−5109.

(6) Zhang, X.; Liu, W.; Wei, G. Z.; Banerjee, D.; Hu, Z.; Li, J. Systematic Approach in Designing Rare-Earth-Free Hybrid Semiconductor Phosphors for General Lighting Applications. *J. Am. Chem. Soc.* **2014**, *136*, 14230−14236.

(7) Shaikh, R. N.; Anis, M.; Gambhire, A. B.; Shirsat, M. D.; Hussaini, S. S. Growth, optical and dielectric studies of glycine doped ammonium dihydrogen phosphate NLO crystal: potential material for optoelectronics applications. *Mater. Res. Express* **2014**, *1*, No. 015016.

(8) Danel, A.; Wojtasik, K.; Szlachcic, P.; Gryl, M.; Stadnicka, K. A New Regiospecific Synthesis Method of 1H-Pyrazolo[3,4-b]-Quinoxalines − Potential Materials for Organic Optoelectronic Devices, and a Revision of an Old Scheme. *Tetrahedron* **2017**, *73*, 5072−5081.

(9) Kurtz, S. K.; Perry, T. T. A Powder Technique for the Evaluation of Nonlinear Optical Materials. *J. Appl. Phys.* **1968**, *39*, 3798−3813.

(10) Dougherty, J. P.; Kurtz, S. K. A second harmonic analyzer for the detection of non-centrosymmetry. *J. Appl. Crystallogr.* **1976**, *9*, 145−158.

(11) *International Tables for Crystallography Volume D: Physical properties of crystals*; Authier, A., Ed.; Kluwer Academic Publishers: Dordrecht/Boston/London, 2003.

(12) Newnham, R. E. *Properties of Materials. Anisotropy, Symmetry, Structure*; Oxford University Press: New York, 2005.

(13) Gryl, M.; Stadnicka, K. Rubidium 2,4,6-Trioxo-1,3-Diazinan-5-Ide-1,3-Diazinane-2,4,6-Trione-Water (1/1/1). *Acta Crystallogr., Sect. E: Struct. Rep. Online* **2011**, *67*, m571−m572.

(14) Ennaceur, N.; Ledoux-Rak, I. Reinvestigation of the crystal structure, vibrational spectroscopic studies and DFT calculations of 4, 4′-bipyridinium dinitrate: An efficient SHG material for electro-optic devices. *J. Phys. Chem. Solids* **2018**, *120*, 223−230.

(15) Owczarek, M.; Miniewicz, A.; Szklarz, P.; Jakubas, R. Crystal structures and related to noncentrosymmetricity properties of 4-aminomorpholinium salts. *Chem. Phys. Lett.* **2016**, *665*, 31−35.

(16) Moskwa, M.; Bator, G.; Rok, M.; Medycki, W.; Miniewicz, A.; Jakubas, R. Investigations of organic−inorganic hybrids based on homopiperidinium cation with haloantimonates(III) and halobismuthates(III). Crystal structures, reversible phase transitions, semiconducting and molecular dynamic properties. *Dalton Trans.* **2018**, *47*, 13507−13522.

(17) Gryl, M.; Seidler, T.; Wojnarska, J.; Stadnicka, K. M.; Matulkova, I.; Němec, I.; Němec, P. Co-Crystals of 2-Amino-5-Nitropyridine Barbital with Extreme Birefringence and Large Second Harmonic Generation Effect. *Chem. − Eur. J.* **2018**, *24*, 8727−8873.

(18) Liu, X.; Ji, C.; Wu, Z.; Li, L.; Han, S.; Wang, Y.; Sun, Z.; Luo, J. [C$_5$H$_{12}$N]SnCl$_3$: A Tin Halide Organic−Inorganic Hybrid as an Above-Room-Temperature Solid-State Nonlinear Optical Switch. *Chem. − Eur. J.* **2019**, *25*, 2610−2615.

(19) Athmani, H.; Kijatkin, C.; Benali-Cherif, R.; Pillet, S.; Schaniel, D.; Imlau, M.; Benali-Cherif, N.; Bendeif, E.-E. Nonlinear optical organic−inorganic crystals: synthesis, structural analysis and verification of harmonic generation in tri-(o-chloroanilinium nitrate). *Acta Crystallogr., Sect. B: Struct. Sci., Cryst. Eng. Mater.* **2019**, *75*, 107−114.

(20) Chen, X.-G.; Zhang, Y.-Z.; Sun, D.-S.; Gao, J.-X.; Hua, X.-N.; Liao, W.-Q. Above room-temperature dielectric and nonlinear optical switching materials based on [(CH$_3$)$_3$S]$_2$[MBr$_4$] (M = Cd, Mn and Zn). *Dalton Trans.* **2019**, *48*, 11292−11297.

(21) Kamatchi, K.; Umarani, P.; Radhakrishnan, T.; Ramachandra Raja, C. Investigation on organic-inorganic hybrid NLO crystal L-Valine Potassium Penta Borate octa hydrate (LVPPB) for NLO applications. *Optik* **2018**, *172*, 674−679.

(22) Gryl, M.; Kozieł, M.; Stadnicka, K.; Matulková, I.; Němec, I.; Tesařová, N.; Němec, P. Lidocaine Barbiturate: A Promising Material for Second Harmonic Generation. *Cryst. Eng. Comm.* **2013**, *15*, 3275−3278.

(23) Gryl, M.; Cenedese, S.; Stadnicka, K. Crystal Engineering and Charge Density Study of Pharmaceutical Nonlinear Optical Material: Melamine-Barbital Co-Crystal. *J. Phys. Chem. C* **2015**, *119*, 590−598.

(24) Zheng, X.; Shi, P.-P.; Lu, Y.; Zhou, L.; Gao, J.-X.; Geng, F.-J.; Wu, D.-H.; Fu, D.-W.; Ye, Q. Dielectric and nonlinear optical dual switching in an organic-inorganic hybrid relaxor [(CH$_3$)$_3$PCH$_2$OH]-[Cd(SCN)$_3$]. *Inorg. Chem. Front.* **2017**, *4*, 1445−1450.

(25) Kosuge, H.; Okada, S.; Oikawa, H.; Nakanishi, H. Preparation of Pyridinium Iodide-CdI$_2$ Hybrids for Nonlinear Optical Materials. *Supramol. Chem.* **2001**, *13*, 233−245.

(26) Zhai, Q.-G.; Gao, X.; Li, S.-N.; Jiang, Y.-C.; Hu, M.-C. Solvothermal synthesis, crystal structures and photoluminescence properties of the novel Cd/X/α,ω-bis(benzotriazole)alkane hybrid family (X = Cl, Br and I). *CrystEngComm* **2011**, *13*, 1602−1616.

(27) Chang, X.-H.; Li, S.-H.; Du, D.-G. Crystal structure of catena-poly[hexakis(μ2-chlorido)-hexakis(4-(1H-pyrazol-5-yl)pyridine-κN)-tricadmium(II)], Cd$_3$C$_{48}$H$_{42}$Cl$_6$N$_{18}$. *Z. Kristallogr.* **2017**, *232*, 261−263.

(28) Chen, X.-Y.; Zhang, N.-N.; Cai, L.-Z.; Li, P.-X.; Wang, M.-S.; Guo, G.-C. N-Methyl-4-pyridinium Tetrazolate Zwitterion-Based Photochromic Materials. *Chem. − Eur. J.* **2017**, *23*, 7414−7417.

(29) Park, I.-H.; Kim, J.-Y.; Kim, K.; Lee, S. S. Homonuclear and Heteronuclear Complexes of Calix[4]-bis-monothiacrown-5 with Oligomer and Polymer Structures. *Cryst. Growth Des.* **2014**, *14*, 6012−6023.

(30) Rogers, R. D.; Bond, A. H.; Aguinaga, S. Synthesis and crystallographic characterization of [Cd(OH$_2$)$_2$ (μ-Br)$_4$ (Cd(2-hydroxyethyl sulfide) (μ-Br)$_2$]$_n$. *J. Crystallogr. Spectrosc. Res.* **1993**, *23*, 857−862.

(31) Samai, S.; Biradha, K. Coordination Polymers of Flexible Bis(benzimidazole) Ligand: Halogen Bridging and Metal⋯Arene Interactions. *Cryst. Growth Des.* **2011**, *11*, 5723−5732.

(32) Santra, A.; Mondal, G.; Acharjya, M.; Bera, P.; Panja, A.; Mandal, T. K.; Mitra, P.; Bera, P. Catechol oxidase mimetic activity of copper(I) complexes of 3,5-dimethyl pyrazole derivatives: Coordina-

tion behavior, X-ray crystallography and electrochemical study. *Polyhedron* **2016**, *113*, 5−15.

(33) Wu, C.-D.; Hu, A.; Zhang, L.; Lin, W. A Homochiral Porous Metal−Organic Framework for Highly Enantioselective Heterogeneous Asymmetric Catalysis. *J. Am. Chem. Soc.* **2005**, *127*, 8940−8941.

(34) Wojnarska, J.; Gryl, M.; Seidler, T.; Rydz, A.; Oszajca, M.; Stadnicka, K. M.; Marzec, M.; Matulková, I.; Němec, I.; Němec, P. Crystal Structure and (Non)linear Optical Properties of a Cyanuric Acid Isoniazid <1/1> Co-crystal: Shortcomings of Phase Matching Determination from Powdered Samples. *Cryst. Growth Des.* **2019**, *19*, 6831−6836.

(35) Suponitsky, K. Y.; Timofeeva, T. V.; Antipin, M. Y. Molecular and crystal design of nonlinear optical organic materials. *Russ. Chem. Rev.* **2006**, *75*, 457−496.

(36) Costin-Hogan, C. E.; Chen, C.-L.; Hughes, E.; Pickett, A.; Valencia, R.; Rath, N. P.; Beatty, A. M. "Reverse" engineering: Toward 0-D cadmium halide clusters. *CrystEngComm* **2008**, *10*, 1910−1915.

(37) Altomare, A.; Camalli, M.; Cuocci, C.; Giacovazzo, C.; Moliterni, A.; Rizzi, R. EXPO2009: structure solution by powder data in direct and reciprocal space. *J. Appl. Crystallogr.* **2009**, *42*, 1197−1202.

(38) Altomare, A.; Campi, G.; Cuocci, C.; Eriksson, L.; Giacovazzo, C.; Moliterni, A.; Rizzi, R.; Werner, P.-E. Advances in powder diffraction pattern indexing: N-TREOR09. *J. Appl. Crystallogr.* **2009**, *42*, 768−775.

(39) Favre-Nicolin, V.; Černý, R. FOX, 'free objects for crystallography': a modular approach to *ab initio* structure determination from powder diffraction. *J. Appl. Crystallogr.* **2002**, *35*, 734−743.

(40) Petricek, V.; Dusek, M.; Palatinus, L. Crystallographic computing system JANA2006: general features. *Z. Kristallogr. Cryst. Mater.* **2014**, *229*, 345−352.

(41) Rietveld, H. M. A profile refinement method for nuclear and magnetic structures. *J. Appl. Crystallogr.* **1969**, *2*, 65−71.

(42) Loopstra, B. O.; Rietveld, H. M. Further refinement of the structure of WO$_3$. *Acta Crystallogr., Sect. B: Struct. Crystallogr. Cryst. Chem.* **1969**, *25*, 1420−1421.

(43) Loopstra, B. O.; Rietveld, H. M. The structure of some alkaline-earth metal uranates. *Acta Crystallogr., Sect. B: Struct. Crystallogr. Cryst. Chem.* **1969**, *25*, 787−791.

(44) Otwinowski, Z.; Minor, W. *Processing of X-ray Diffraction Data Collected in Oscillation Mode in Methods in Enzymology*; Carter, C. W., Jr.; Sweet, R. M., Eds.; Academic Press: New York, 1997; *276*, pp 307−326.

(45) Altomare, A.; Burla, M. C.; Camalli, M.; Cascarano, G. L.; Giacovazzo, C.; Guagliardi, A.; Moliterni, A. G. G.; Polidori, G.; Spagna, R. SIR97: a new tool for crystal structure determination and refinement. *J. Appl. Crystallogr.* **1999**, *32*, 115−119.

(46) Sheldrick, G. M. Crystal structure refinement with SHELXL. *Acta Crystallogr., Sect. C: Struct. Chem.* **2015**, *71*, 3−8.

(47) Farrugia, L. J. WinGX suite for small-molecule single-crystal crystallography. *J. Appl. Crystallogr.* **1999**, *32*, 837−838.

(48) *Powder Diffraction File − PDF-4+*; International Crystal Structure Database; Pennsylvania, U.S.A., 2020.

(49) Dovesi, R.; Erba, A.; Orlando, R.; Zicovich-Wilson, C. M.; Civalleri, B.; Maschio, L.; Rerat, M.; Casassa, S.; Baima, J.; Salustro, S.; Kirtman, B. Quantum-mechanical condensed matter simulations with CRYSTAL. *WIREs Comput. Mol. Sci.* **2018**, *8*, No. e1360.

(50) Dovesi, R.; Saunders, V. R.; Roetti, C.; Orlando, R.; Zicovich-Wilson, C. M.; Pascale, F.; Civalleri, B.; Doll, K.; Harrison, N. M.; Bush, I. J.; D'Arco, P.; Llunell, M.; Causà, M.; Noël, Y.; Maschio, L.; Erba, A.; Rerat, M.; Casassa, S. *CRYSTAL17 User's Manual*; University of Torino: Italy, 2017.

(51) (a) Seidler, T.; Stadnicka, K.; Champagne, B. Linear and second-order nonlinear optical properties of ionic organic crystals. *J. Chem. Phys.* **2014**, *141*, 104109. (b) Seidler, T.; Stadnicka, K.;

Champagne, B. Erratum:"Linear and second-order nonlinear optical properties of ionic organic crystals". *J. Chem. Phys.* **2015**, *142*, 239901.

(52) Seidler, T.; Krawczuk, A.; Champagne, B.; Stadnicka, K. QTAIM-Based Scheme for Describing the Linear and Nonlinear Optical Susceptibilities of Molecular Crystals Composed of Molecules with Complex Shapes. *J. Phys. Chem. C* **2016**, *120*, 4481−4494.

(53) Munn, R. W. Microscopic Dielectric Theory for Molecular Crystals. *J. Chem. Phys.* **1980**, *50*, 119−126.

(54) Bounds, P. J.; Munn, R. W. Polarization Energy of a Localized Charge in a Molecular Crystal.II. Charge-Quadrupole Energy. *J. Chem. Phys.* **1981**, *59*, 41−45.

(55) Hurst, M.; Munn, R. W. Theory of Molecular Opto-Electronics. I. Macroscopic and Microscopic Response. *J. Mol. Electron.* **1986**, *2*, 35−41.

(56) Frisch, M. J.; Trucks, G. W.; Schlegel, H. B.; Scuseria, G. E.; Robb, M. A.; Cheeseman, J. R.; Scalmani, G.; Barone, V.; Petersson, G. A.; Nakatsuji, H.; Li, X.; Caricato, M.; Marenich, A. V.; Bloino, J.; Janesko, B. G.; Gomperts, R.; Mennucci, B.; Hratchian, H. P.; Ortiz, J. V.; Izmaylov, A. F.; Sonnenberg, J. L.; Williams-Young, D.; Ding, F.; Lipparini, F.; Egidi, F.; Goings, J.; Peng, B.; Petrone, A.; Henderson, T.; Ranasinghe, D.; Zakrzewski, V. G.; Gao, J.; Rega, N.; Zheng, G.; Liang, W.; Hada, M.; Ehara, M.; Toyota, K.; Fukuda, R.; Hasegawa, J.; Ishida, M.; Nakajima, T.; Honda, Y.; Kitao, O.; Nakai, H.; Vreven, T.; Throssell, K.; Montgomery, J. A., Jr.; Peralta, J. E.; Ogliaro, F.; Bearpark, M. J.; Heyd, J. J.; Brothers, E. N.; Kudin, K. N.; Staroverov, V. N.; Keith, T. A.; Kobayashi, R.; Normand, J.; Raghavachari, K.; Rendell, A. P.; Burant, J. C.; Iyengar, S. S.; Tomasi, J.; Cossi, M.; Millam, J. M.; Klene, M.; Adamo, C.; Cammi, R.; Ochterski, J. W.; Martin, R. L.; Morokuma, K.; Farkas, O.; Foresman, J. B.; Fox, D. J. *Gaussian 16, Rev. C.01*; Gaussian, Inc.: Wallingford, CT, 2016.

(57) Todd, A. K. *AIMAll (Version 19.10.12)*; TK Gristmill Software: Overland Park KS, USA, 2019; aim.tkgristmill.com.

(58) He, G. S. *Nonlinear Optics and Photonics. Chapter 3. Second-Order Nonlinear (Three-Wave) Frequency Mixing*; Oxford University Press, 2015.

(59) Southgate, P. D.; Hall, D. S. Anomalously high nonlinear optical effects in m-nitroaniline. *Appl. Phys. Lett.* **1971**, *18*, 456−458.

(60) Radhakrishnan, T. P. Molecular Structure, Symmetry, and Shape as Design Elements in the Fabrication of Molecular Crystals for Second Harmonic Generation and the Role of Molecules-in-Materials. *Acc. Chem. Res.* **2008**, *41*, 367−376.

(61) Vijayan, N.; Bhagavannarayana, G.; Ramesh, K. R.; Gopalakrishnan, R.; Maurya, K. K.; Ramasamy, P. A Comparative study on solution and Bridgman grown single crystals of benzimidazole by high-resolution XRD, FTIR, microhardness, laser damage threshold and SHG measurements. *Cryst. Growth Des.* **2006**, *6*, 1542−1546.

(62) Rok, M.; Zarychta, B.; Bil, A.; Trojan-Piegza, J.; Medycki, W.; Miniewicz, A.; Piecha-Bisiorek, A.; Cizman, A.; Jakubas, R. A multiaxial electrical switching in a one-dimensional organic−inorganic (pyrrolidinium)$_2$Cd$_2$I$_6$ ferroelectric and photoluminescent crystal. *J. Mater. Chem. C* **2021**, *9*, 7665−7676.